ELSEVIER

Materials Science and Engineering A254 (1998) 13–32

MATERIALS SCIENCE & ENGINEERING A

A mathematical model for the dissolution kinetics of Mg_2Si-phases in Al–Mg–Si alloys during homogenisation under industrial conditions

Fred Vermolen [a,b], Kees Vuik [b], Sybrand van der Zwaag [a,*]

[a] *Laboratory for Materials Science, Delft University of Technology, Delft, The Netherlands*
[b] *Faculty of Technical Mathematics and Informatics, Delft University of Technology, Delft, The Netherlands*

Received 21 January 1998; received in revised form 29 May 1998

Abstract

A numerical analysis of the homogenisation treatment of aluminium alloys under industrial circumstances is presented. The basis of this study is a mathematical model which is applicable to the dissolution of stoichiometric multicomponent phases in both finite and infinite ternary media. It handles both complete and incomplete particle dissolution as well as the subsequent homogenisation of the matrix. The precipitate volume fraction and matrix homogeneity are followed during the entire homogenisation treatment. First, the influence of the metallurgical parameters, such as particle size distribution, initial matrix concentration profile and particle geometry on the dissolution- and matrix homogeneity kinetics is analysed. Then, the impact of the heating-rate and local temperature on the homogenisation kinetics is investigated. Conclusions for an optimal homogenisation treatment of aluminium alloys may be drawn. The model presented is general but the calculations were performed for the system Al–Mg–Si with an Al-rich matrix and Mg_2Si-precipitates.

Keywords: Particle dissolution; Homogenisation; Aluminium alloys; Mg_2Si

1. Introduction

The as-cast microstructure of commercial AlMgSi-alloys contains many inhomogeneities such as segregation (concentration gradients), secondary phases and grain size variations. These secondary phases may be present as needle-shaped Al–Fe–Mg–Si compounds or as Mg_2Si-phases. Due to these inhomogeneities the mechanical properties may vary greatly throughout the alloy. This variation in microstructure and local composition may cause heat cracking or other material failures during hot-extrusion of billets of such extrusion alloys.

To prevent this material failure during hot-extrusion and to facilitate the extrusion process, the as-cast alloys are annealed at a temperature just below their eutectic temperature. This thermal treatment, called the homogenisation treatment, aims at the elimination of the microstructural segregation in the AlMgSi-alloy. Stable needle-shaped precipitates may transform into more rounded particles and unstable secondary phases may dissolve partly or entirely. Using thermodynamic models, it is possible to predict the equilibrium of all phases in the microstructure of the alloy at the end of the homogenisation treatment. However, these models cannot be used to predict the rate at which the microstructural changes occur. The present study comprises an analysis of the rate at which the most important secondary phases in Al-extrusion alloys, Mg_2Si-phases, dissolve under industrial circumstances.

To describe this particle dissolution in solid binary alloys several physical models have been developed,

* Corresponding author. Tel.: +31 15 2782248; fax: +31 15 2786730; e-mail: S.vanderZwaag@stm.tudelft.nl

0921-5093/98/ - see front matter
PII S0921-5093(98)00763-1

incorporating the effects of long-distance diffusion [1–5] and non-equilibrium conditions at the interface [6–9]. These models do not consider the technologically important dissolution of stoichiometric multicomponent particles in ternary alloys.

The phase transformations in iron-based ternary alloys have been studied in Refs. [10,11]. Hubert et al. [12] considered the precipitation of stoichiometric MnS and AlN compounds in steels. Their analysis was carried out to predict the size of the precipitates during hot-rolling of steel. The dissolution of Mg_2Si-particles in aluminium alloys has been studied mainly experimentally [13–15]. Reiso et al. [13] compared their results to a simple dissolution model for dissolving particles in infinite media. Kaneko et al. [14] analysed the amount of Mg_2Si-precipitates present in aluminium for different thermal treatments. Their observations were based on measurements of electrical resistivity during the thermal profile. Lodgård et al. [15] analysed precipitation using electrical resistivity measurements as well. Moreover they analysed the complex precipitation sequence of Mg_2Si in aluminium. The influence of the particle stoichiometry, geometry, composition and ratio of the diffusivities of both alloying elements was studied numerically in Ref. [16]. That model has also been used for the determination of the simultaneous dissolution kinetics of a particle and a layer of a secondary intermetallic phase at the grain boundary and the subsequent homogenisation of the matrix in terms of vanishing concentration gradients [17].

However, apart from Hubert's study [12], in none of these studies was the influence of the temperature gradients in the furnace on the kinetics of the dissolution of secondary phases during the heat treatment investigated explicitly. Moreover, the matrix homogeneity during and after the secondary phase dissolution and the effects of the presence of initial concentration gradients in the matrix prior to the heat treatment were not investigated in either of these studies. The present paper takes into account all these parameters and can be used to determine the effects of the grain–particle size distribution, heat-up rate, homogenisation temperature and initial concentration profiles on the dissolution rates of the secondary phases as well as on the subsequent homogenisation of the matrix.

The model assumptions will be briefly described in the next section which deals with the physical definition of the problem, its mathematical formulation and the numerical solution procedure. Subsequently, the results of the calculations will be shown to reveal the influence of some industrial parameters. Finally, some conclusions will be drawn from the calculations.

2. The model

Consider a ternary AlMgSi-alloy as a collection of unequally sized Al-rich grains each surrounded by a layer of Mg_2Si along the grain boundary. To reduce this to a one-dimensional problem the grains are assumed to be spherical. The logarithm of the radius of the grain is assumed to be normally divided [3,18–20]. Hence the probability density function for the grain radius M_2 is:

$$F(M_2, \mu, \sigma^2) = \frac{1}{\sqrt{2\pi}\ln(\sigma)M_2} \times \exp\left(-\frac{(\ln(M_2)-\ln(\mu))^2}{2(\ln(\sigma))^2}\right). \quad (1)$$

Here μ and σ represent the geometric mean and S.D. of the grain radius, respectively. The probability density function of the grain size is subsequently divided into n discrete classes to facilitate later calculations. From a mathematical analysis of the discretisation of the continuous distribution function with equal class widths $\Delta M_2 = \hat{M}_2/n$, with $\hat{M}_2$ the upper bound of the confidence interval of 0.99 (i.e. $\int_0^{\hat{M}_2} F(M_2, \mu, \sigma^2)\,\mathrm{d}M_2 = 0.99$), it appeared that the discretisation error was negligible for $n \geq 20$. The Mg_2Si-layer thickness for each grain radius M_2 was chosen such that the average concentration of the two alloying elements Mg and Si is identical for all grains. Moreover, the initial concentration of Mg and Si in the matrix of each grain were taken to be uniform for all grains. In each grain, containing a Mg_2Si-compound layer at the grain boundary, the diffusion equation (Fick's second law) is solved and the rate of dissolution is calculated accordingly. After the dissolution of a layer, the kinetics of the subsequent flattening of the concentration profile is calculated too.

Mathematically, second phase dissolution in solid state alloys is considered as a diffusion problem with a moving boundary, i.e. a Stefan problem. Second phase dissolution is assumed to proceed sequentially by the decomposition of the (intermetallic) compound, the crossing of the interface and long-range diffusion by the solute atoms. For the cases considered in this paper it is assumed that diffusion is very sluggish relative to the preceding steps, from which it follows that diffusion determines the rate of secondary phase dissolution and local (thermodynamic) equilibrium is maintained at the moving boundary at all stages during dissolution. Hence, a Dirichlet boundary condition applies at the moving particle–matrix interface.

2.1. The underlying mathematical assumptions for each grain

Each grain is considered as a system with a second phase consisting of two chemical elements at the grain

boundary of an Al-rich matrix in which the chemical elements of the compound are partially soluble. The initial concentration in the matrix of alloying element p is $c_p^0(r)$ and the concentration of alloying element p in the secondary phase is denoted as c_p^{part}. When the temperature is increased dissolution of the secondary phase sets in, if $c_p^{\text{part}} > c_p[S(t), t] > c_p^0[S(0)]$, where $c_p[S(t), t]$ is the equilibrium condition of element p at the moving interface $S(t)$.

Within the surrounding matrix in which the diffusion takes place, $G(t)$, at all times the concentration of alloying element p at distance r from the grain centre at time t, $c_p(r, t)$, satisfies the one-dimensional diffusion equation ($a = 0$ for planar geometry, $a = 1$ for cylindrical geometry, $a = 2$ for spherical geometry):

$$\frac{\partial c_p(r,t)}{\partial t} = \frac{D_p(T)}{r^a}\frac{\partial}{\partial r}\left\{ r^a \frac{\partial c_p(r,t)}{\partial r}\right\}$$
$$\forall (r,t) \in G(t) \times \langle 0, t_{\max}\rangle, \tag{2}$$

where $D_p(T)$ denotes the temperature dependent diffusion coefficient of the alloying element through the matrix and $t_{\max}$ is the maximum time considered. The above equation is valid for both the situation when the particle is present and the situation when the particle is fully dissolved. For the case of a dissolving secondary phase at the grain boundary, we have $G(t) = \{r \in R | 0 \le r \le S(t) \le M_2\}$ and for the case of a dissolving particle in the grain centre, we have $G(t) = \{r \in R | 0 \le S(t) \le r \le M_2\}$. M_2 represents the grain boundary. The grain centre $r = 0$ is indicated by M_1. For $c_p(r, t)$ continuous at least up to the second derivative with respect to r in $G(t)$ and the first derivative of t, the solution of Eq. (2) with appropriate boundary and initial conditions is unique. It has been proven by Protter and Weinberger [21] that solutions of Eq. (2) satisfy the maximum principle, i.e. the global extremes of $c_p(r, t)$ either occur at the boundaries and/or for $t = 0$. In the calculations, for which the results are presented here, the matrix material is taken to be Al, which has a partial solubility for Mg and Si, and the compound layer is taken to be composed of Mg_2Si. The binary diffusion coefficients of Si and Mg in Al are taken, respectively, from Fujikawa [22] and Yamane [23]. The cross-diffusion coefficients, as well as the dependency of the diffusion coefficients on the concentration, are neglected for lack of knowledge about these parameters.

In the calculations the initial Mg and Si concentrations in the matrix have been varied. The initial concentrations are taken to be uniform, unless stated otherwise. The concentration profiles in the matrix at the start of the calculation, $G(0)$, need not be uniform but may vary with position as:

$$c_p(r, 0) = c_p^0(r) \quad \forall r \in G(0). \tag{3}$$

In the later stages of the homogenisation process, the secondary phase can get fully dissolved. Hence, $S(\text{it})$ coincides with the outer cell boundary M_2 or with the grain centre $M_1 = 0$, respectively, for the case of a dissolving secondary phase layer at the grain boundary and a dissolving particle at the grain centre. No flux of either alloying elements is assumed through a fixed boundary, resulting in a homogeneous Neumann boundary condition at a fixed boundary (which may either be the centre and/or the outer boundary):

$$\frac{\partial c_p(M_m, t)}{\partial r} = 0 \quad \forall t \in \langle 0, t\rangle,\ m \in \{1, 2\}. \tag{4}$$

If only diffusion in the matrix determines the rate of dissolution, it follows from thermodynamic considerations [16] that, for a stoichiometric Mg_2Si-particle, the concentrations of both alloying elements at the moving Dirichlet boundary, $c_p[S(t), t]$ ($p \in \{\text{Mg, Si}\}$,), are coupled by the following hyperbolic relation:

$$(c_{\text{Si}}[S(t), t])(c_{\text{Mg}}[S(t), t])^2 = K(T) \quad \forall t \in \langle 0, t_{\max}\rangle. \tag{5}$$

The factor $K(T)$ is the solubility product. It depends on temperature according to then Arrhenius relationship.

The interface between the second phase and surrounding matrix, $S(t)$, moves due to the balance of the atoms of alloying element p at the interface. For the case that the second phase remains stoichiometric, this yields the following relationship for the interfacial velocity and interfacial gradients:

$$\frac{\mathrm{d}S(t)}{\mathrm{d}t} = \frac{D_{\text{Si}}}{c_{\text{Si}}^{\text{part}} - c_{\text{Si}}[S(t), t]}\frac{\partial c_{\text{Si}}[S(t), t]}{\partial r}$$
$$= \frac{D_{\text{Mg}}}{c_{\text{Mg}}^{\text{part}} - c_{\text{Mg}}[S(t), t]}\frac{\partial c_{\text{Mg}}[S(t), t]}{\partial r},$$
$$\text{provided that } c_p^{\text{part}} - c_p[S(t), t] \neq 0,\ \forall t \in \langle 0, t_{\max}\rangle. \tag{6}$$

The above set of equations, Eqs. (2)–(6), constitute a classical Stefan problem [24] which consists of two diffusion problems with coupled Dirichlet conditions at the moving boundary. We thus have to find two concentration profiles $c_p(r, t)$ such that Eqs. (2)–(6) are satisfied at all times.

2.2. The numerical solution procedure

Various numerical methods for solving Stefan problems are known. Crank [24] roughly distinguishes three types of methods: the front-tracking, front fixing and fixed-domain methods. In this paper a front tracking method is applied.The algorithm for each time-step is summarised as follows: For the interfacial concentration of one alloying element, say $c_{\text{Mg}}[S(t), t]$, a starting value is chosen: $c_{\text{Mg}}^0[S(0)] < c_{\text{Mg}}[S(t), t] \ll c_{\text{Mg}}^{\text{part}}$. The interfacial concentration of the other alloying element,

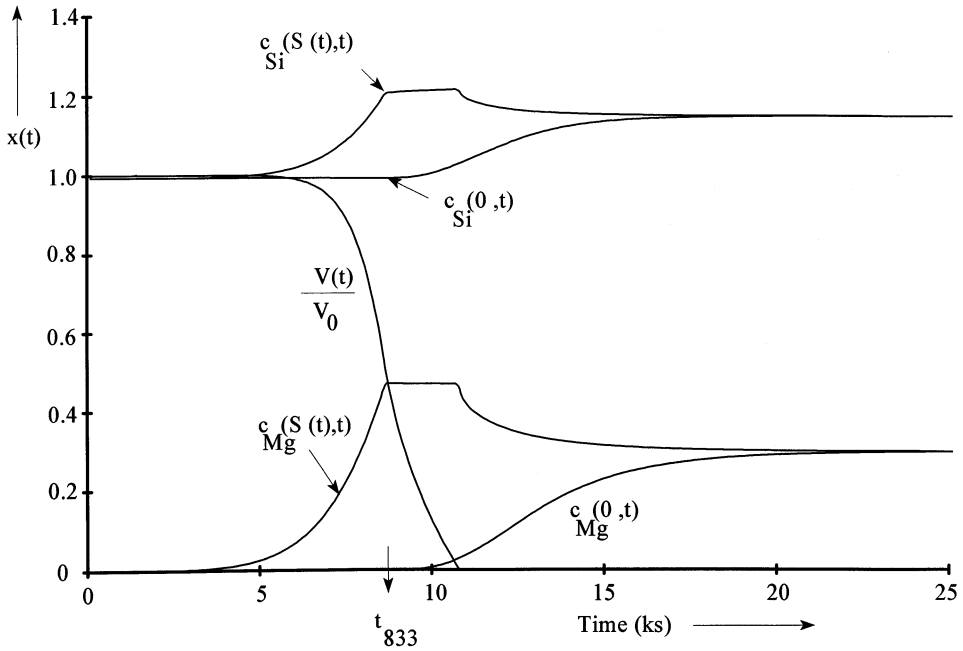

Fig. 1. The normalised volume fraction of the Mg_2Si-layer, the concentrations (in mass%) at the moving boundary, $c_p[S(t), t]$, and grain centre, $c_p(0, t)$, of both alloying elements. The homogenisation temperature was reached at $t_{833} = 8.66$ ks. $V(t)$ and V_0 correspond to the volume of the Mg_2Si-layer at time t and to the initial volume of the Mg_2Si-layer, respectively.

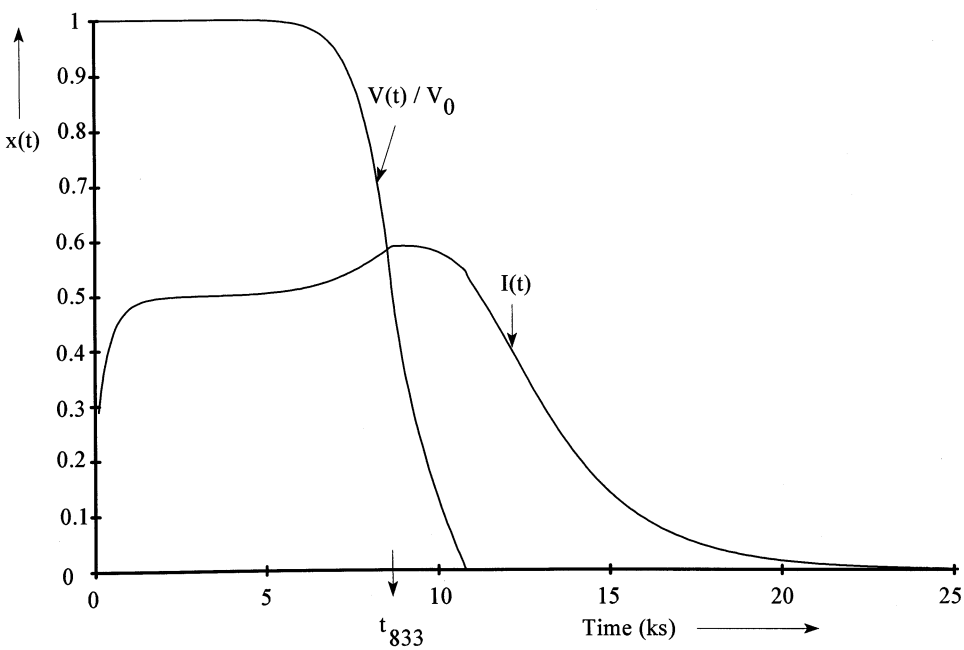

Fig. 2. The evolution of the normalised Mg_2Si volume and the inhomogeneity parameter as a function of time. t_{833} Indicates the time at which the homogenisation temperature of 833 K ($t_{833} = 8.66$ ks) was reached.

(corresponding to a Mg_2Si thickness of 0.254×10^{-6} m).

The results for the dissolution kinetics and the inhomogeneity parameter for this reference system are shown in Figs. 1 and 2. Fig. 1 indicates the behaviour of the normalised Mg_2Si volume, the concentrations of Mg and Si at the moving boundary between the Mg_2Si-layer and the matrix and the concentrations of both alloying elements at the grain centre. $V(t)$ and V_0 correspond to the volume of the Mg_2Si-layer at time t and to the initial volume of the Mg_2Si-layer, respectively.

At the very early stages, as shown in Fig. 1, hardly anything happens; all parameters remain constant. This is due to the very low concentration gradients (resulting from a low solubility product) and low diffusion coeffi-

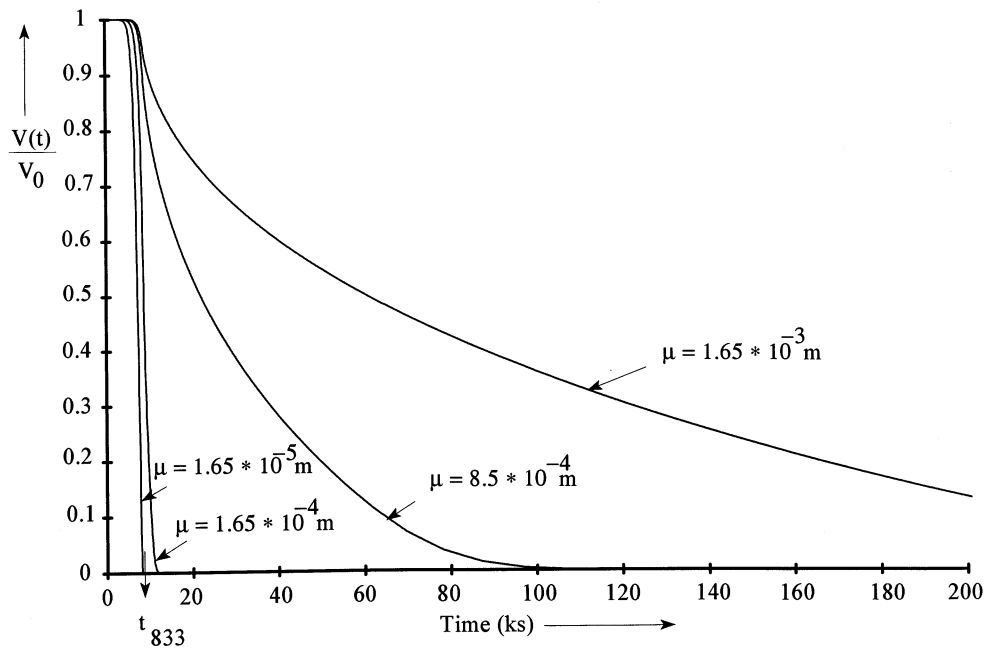

Fig. 3. The influence of the geometric mean of the grain size on the dissolution kinetics of a spherical layer of Mg_2Si. The geometric S.D. is 1.1. $t_{833} = 8.66$ ks Indicates the time at which the homogenisation temperature of 833 K was reached.

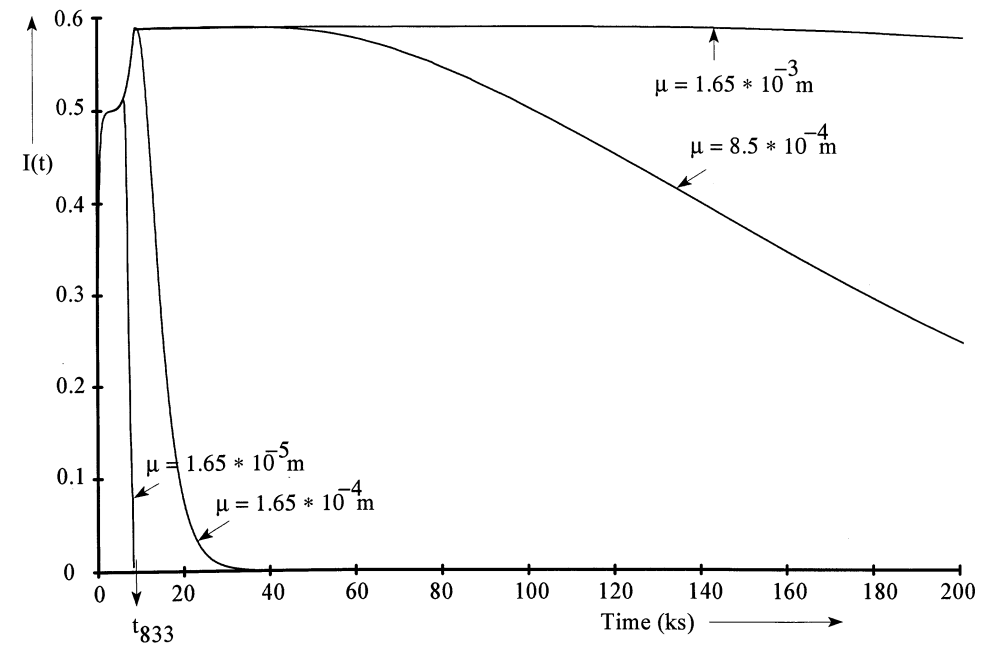

Fig. 4. The influence of the geometric mean of the grain size on the evolution of the inhomogeneity parameter in case of dissolution of a spherical Mg_2Si-layer. The geometric S.D. is 1.1. The homogenisation temperature was reached after $t_{833} = 8.66$ ks.

cients at the lower temperatures. From Eq. (6) it then follows that the displacement of the moving boundary is approximately zero. As the temperature increases, the solubility product and diffusion coefficients increase too. Then, the interfacial concentrations start to increase and the Mg_2Si-compound layer starts to dissolve. The atoms that diffuse from the compound layer into the grain have not reached the grain centre yet, so the concentrations at the grain centre remain equal to the initial concentrations. When the temperature has reached the homogenisation temperature, the concentrations at the moving boundary remain almost constant and a discontinuity of the derivative in the interfacial concentrations results at the moment of temperature fixation. As the layer dissolution proceeds, the atoms from the compound layer start to reach the grain centre and accumulate there. Hence the concentrations of the alloying elements at the grain centre start to

increase. Due to a larger diffusivity of Si at 833 K, the Si atoms accumulate at the grain centre before the Mg atoms do. At a later stage, $t = 11$ ks, the compound layer dissolves entirely $[S(t) = M_2]$ and the Dirichlet condition at the moving boundary changes into a homogeneous Neumann boundary. Now, the concentrations at this fixed boundary start to decrease, causing a strong discontinuity for the time derivative of the interfacial concentrations. The concentrations at the grain centre are not affected by this discontinuity. At the later stages after the dissolution of the compound layer the concentration profiles flatten and, for each alloying element, the concentrations at the grain centre and the outer grain boundary converge to each other.

Fig. 2 shows the evolution of the normalised Mg_2Si-layer volume and the inhomogeneity parameter as defined in Eq. (7). The inhomogeneity parameter for this case is initially zero as the equilibrium state was used as the starting condition and the initial concentration profiles for both elements were flat. During heating up, the interfacial concentrations of Mg and Si increase, while those at the grain centre remain constant. Hence, $I(t)$ increases during heating up. A mathematical justification of the complex shape of the I(it)-curve, before the maximum $I(t)$ is reached, is given in Appendix A. Just before the accumulation of the atoms from the Mg_2Si-layer at the grain centre, the inhomogeneity parameter is maximal. At that stage the Mg and Si concentrations at the grain centre, respectively, are equal to approximately 0 and 0.993 mass. Hence, the maximum $I(t)$ is equal to about 0.58. It is also clear that Si is more homogeneously distributed in the matrix than Mg.

From Fig. 1 it can be seen that, when the homogenisation temperature is reached, the Mg concentration at the moving boundary stays almost constant but the atoms start to accumulate at the grain centre, hence the matrix becomes more homogeneous and the inhomogeneity parameter starts to decrease. When the particle is fully dissolved, the moving boundary becomes fixed and its Dirichlet boundary condition transforms into a Neumann-condition. Due to the strong discontinuity of the time derivative of the maximum/interfacial concentrations, a small jump in the time derivative of the inhomogeneity parameter can then be observed (the time derivative of the inhomogeneity parameter has a discontinuity). As can be seen from Figs. 1 and 2, the matrix reaches homogeneity a long time (about 14 ks) after the dissolution of the Mg_2Si-layer.

3.2. The effect of the shape of the statistical particle size distribution

Due to the nature of the solidification process, the microstructure may differ over the cross-section of the billet. The differences may be either in solute concentrations or in particle size distribution. Therefore, the influences of the particle size distribution on the dissolution and homogenisation kinetics were investigated. The analysis has been done by variation of the mean grain size and the S.D. of the grain size. To enable direct comparison with the behaviour of the monodisperse reference system, all analyses correspond to the same initial Mg_2Si volume fraction, the same overall alloy concentrations and same time–temperature profiles as in the reference system from the preceding paragraph.

In order to deal with the grain size distribution in a proper way, the definition of the inhomogeneity parameter (Eq. (9)) is adjusted, to yield for a system of n classes:

$$I(t) = \frac{1}{2}\sum_{i=1}^{n}\left[\Psi(M_2^i, \mu, \sigma^2)V_{\mathrm{mat}}^i(t)\sum_{p=\{\mathrm{Mg,Si}\}}\left\{\frac{\max_{r\in G^{i(t)}}(c_p(r,t)) - \min_{r\in G^{i(t)}}(c_p(r,t))}{\max_{r\in G^{i(t)}}(c_p(r,t))}\right\}\right]\Big/\sum_{i=1}^{n}\Psi(M_2^i, \mu, \sigma^2)V_{\mathrm{mat}}^i(t) \qquad (9)$$

In which the matrix domain for grain size class i has been defined as $G^i(t) \equiv \{r \in R \,|\, 0 \le r \le S^i(t) \le M_2^i\}$ and $V_{\mathrm{mat}}^i(t)$ is the volume of $G^i(t)$, i.e. the matrix volume. The function $\Psi(M_2^i, \mu, \sigma^2) \approx F(M_2^i, \mu, \sigma^2)\Delta M_2$ denotes the probability of the occurrence of a particle in size class i, in which the logarithm of the particle size is statistically divided according to a normal distribution. ΔM_2 denotes the class width. In all calculations n was set equal to 20.

The results, obtained for the Mg_2Si-layers surrounding spherical grains, have been plotted in Figs. 3–6. In Figs. 3 and 4 the influence of the geometric mean of the grain size, μ, on the dissolution kinetics and the evolution of the inhomogeneity parameter is shown. Figs. 3 and 4 show that the Mg_2Si dissolution and matrix homogenisation proceed faster for smaller grains, as is to be expected.

During the first stage of the heat-up, the evolution of the inhomogeneity parameter coincides for all geometric means: the initial concentrations are similar and then the evolution of the concentrations at the moving boundary roughly coincides for all systems. At the later stages the evolution of the concentrations at the grain centre starts to differ, and the decrease of $I(t)$ becomes significantly smaller for larger grain sizes.

The influence of the geometric S.D. of the grain size on the dissolution kinetics and inhomogeneity parameter are illustrated in Figs. 5 and 6. For cases of a large S.D. of the grain size, it can be seen that at the later stages the few larger grains significantly delay the dissolution and the evolution of the inhomogeneity parameter.

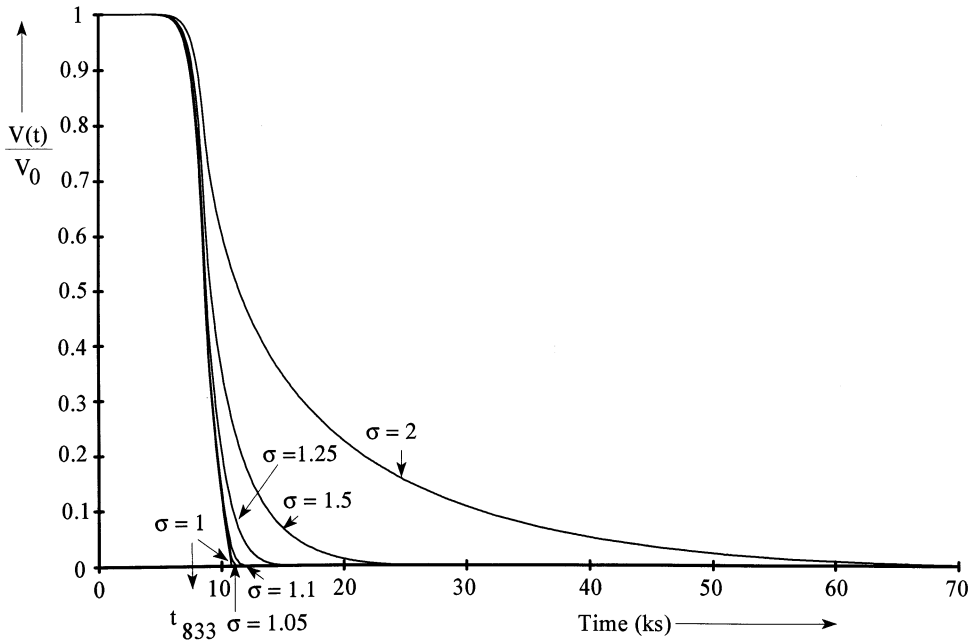

Fig. 5. The evolution of the normalised Mg_2Si-layer volume with time for different geometric S.D. of the grain size. The geometric mean of the grain size is 1.65×10^{-4} m. The homogenisation temperature was reached at $t_{833} = 8.66$ ks.

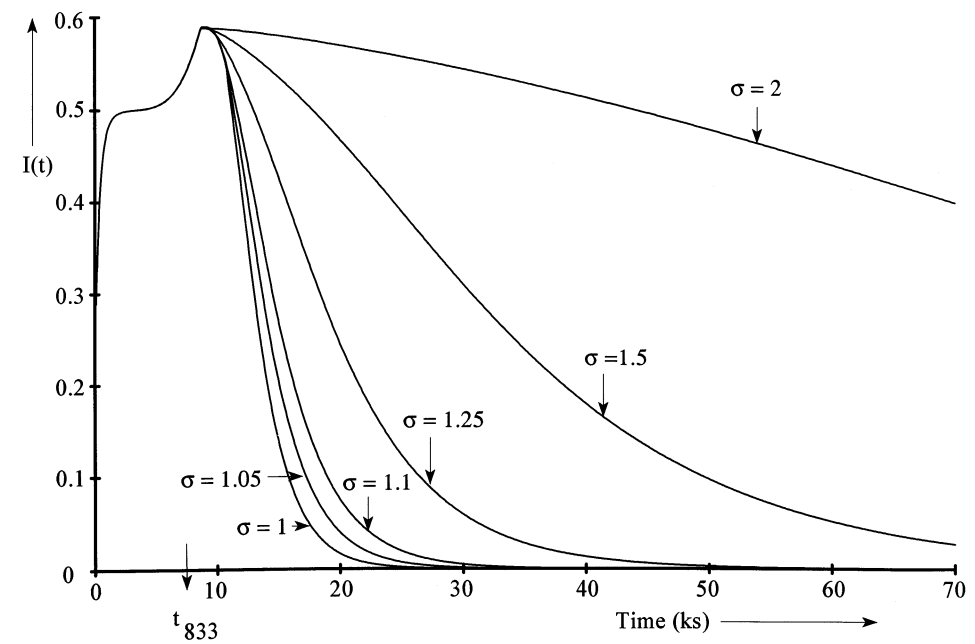

Fig. 6. The influence of the geometric S.D. of the grain size on the evolution of the inhomogeneity parameter in the case of the dissolution of a spherical layer of Mg_2Si. The geometric mean of the grain size is 1.65×10^{-4} m. The homogenisation temperature was reached at $t_{833} = 8.66$ ks.

It can be observed from Figs. 5 and 6 that the time to reach matrix homogeneity after the dissolution of all compound layers is strongly influenced by the geometrical S.D. of the grain size. Moreover, it appears that the ratio between the time to reach matrix homogeneity and the time to dissolve all particles varies non-linearly with the S.D. More formally: If t_1 is the minimal time to dissolve all particles until $V_{\text{prec}}(t_1)/V_{\text{prec}}(0) = \varepsilon$, for an arbitrary real $\varepsilon > 0$, and if t_2 is the minimal time to reach matrix homogeneity, $I(t_2) < \varepsilon$, then it appears that $t_2/t_1 = F(\sigma)$. $F(\sigma)$ has been calculated for $\varepsilon = 0.05$, 0.1 and 0.2, yielding $f(\sigma)$, $g(\sigma)$ and $h(\sigma)$ respectively. Fig. 7 depicts the evolution of $f(\sigma)$, $g(\sigma)$ and of $h(\sigma)$ in the range of $\sigma \in [1, 3]$, in which the geometric mean of the grain size is constant.

Fig. 7 shows that the ratio of the time needed to obtain grain homogeneity and the time needed until the Mg_2Si-layer disappeared is approximately 1.5 and 6 for,

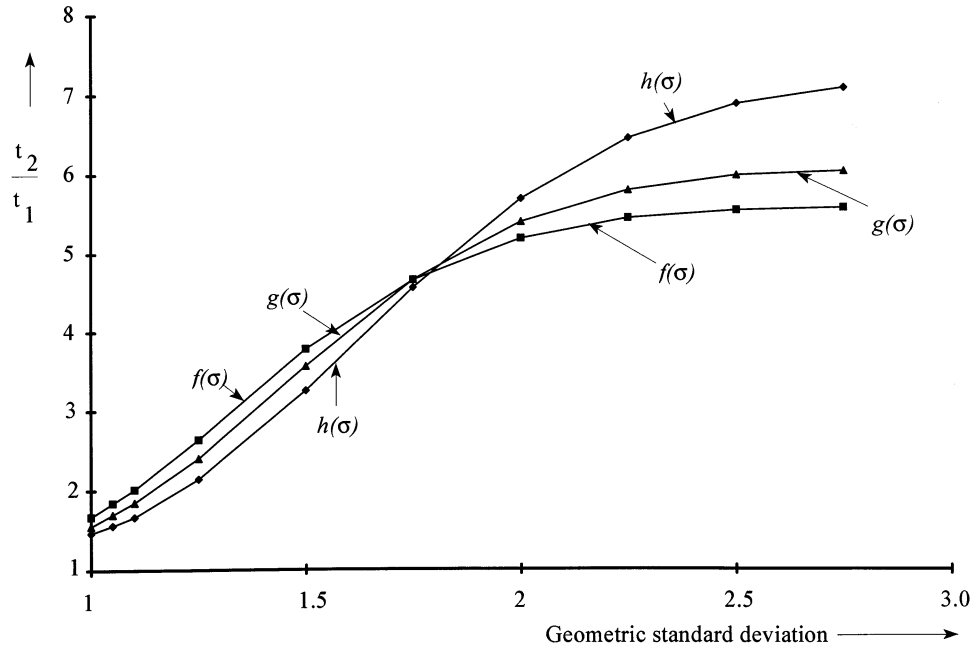

Fig. 7. The evolution of the functions $f(\sigma)$, $g(\sigma)$ and of $h(\sigma)$ as a function of σ for reference conditions specified in the text.

respectively, $\sigma = 1$ and $\sigma = 3$. So for larger geometric S.D. of the grain size the alloy has to be annealed relatively longer after the dissolution of the Mg_2Si-phases to obtain a more homogeneous matrix than for lower geometric S.D. Therefore, it may be concluded that the ratio of the time needed to obtain grain homogeneity and the time to dissolve the Mg_2Si-layer depends strongly on the statistical distribution of the grain size.

3.3. The influence of the initial matrix composition

In the numerical experiments of this section the dissolution kinetics and matrix inhomogeneity has been evaluated for three sets of initial matrix concentrations. In the first set of calculations the initial matrix concentrations are chosen arbitrarily. The second set of calculations correspond to different homogeneous initial matrix compositions but they all correspond to an identical overall composition. The Mg_2Si-layer thickness then has been adjusted accordingly. The third set of calculations apply to a fixed overall composition as well. However, they show the effect of the initial matrix concentration profiles.

Table 1
The values used for the initial matrix concentrations in the first set of calculations with varying initial matrix concentration and the indexing of the curves in Figs. 8 and 9

Curve index	c^0_{Si} (mass%)	c^0_{Mg} (mass%)	$\langle c_{Si} \rangle$ (mass%)	$\langle c_{Mg} \rangle$ (mass%)
I	0	0	0.1615	0.3
II	0.5	0.25×10^{-5}	0.6592	0.3
III	1	0.25×10^{-5}	1.1569	0.3
IV	0	0.5	0.1615	0.7977
V	0	1	0.1615	1.2954
VI	1	1	1.1569	1.2954

3.4. The effect of the arbitrary initial matrix concentrations

In these calculations the initial matrix concentration has been varied. This variation yields a change of the overall concentrations. The conditions used in the first set of calculations are listed in Table 1 while the results are shown in Figs. 8 and 9. The rest of the conditions were identical to those of the reference system.

Curve I in Fig. 8 shows a very fast decreasing volume of the compound layer due to the low initial matrix concentrations. Its corresponding curve I for the inhomogeneity starts at unity and decreases monotonously down to zero. Curves II and III in Fig. 8 correspond to an increasing initial Si matrix concentration and thus to a decreasing dissolution rate. The initial matrix concentration of Mg was taken to be 0.25×10^{-5} mass%. It can be seen that at the initial stages the inhomogeneity parameter increases from zero to 0.5. It then remains at approximately 0.5 for some time, because for Mg the initial concentration is small and therefore its contribution to the inhomogeneity parameter is large. Whereas the initial concentration of Si is large and close to the maximum solubility, its contribution to the inhomogeneity parameter is about zero. Thus, it can then be concluded that the concentration of Mg in the matrix is rather inhomogeneous while the concentration of Si is rather homogeneous.

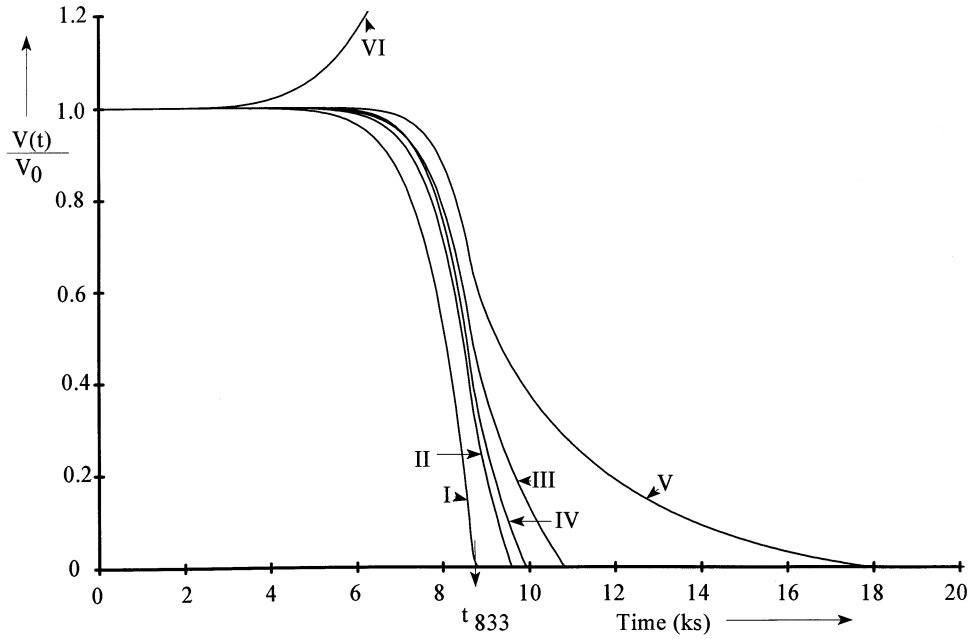

Fig. 8. The dissolution kinetics of a Mg_2Si-layer for different initial concentrations. The curves are explained in the text and in Table 1. The homogenisation temperature was reached at $t_{833} = 8.66$ ks.

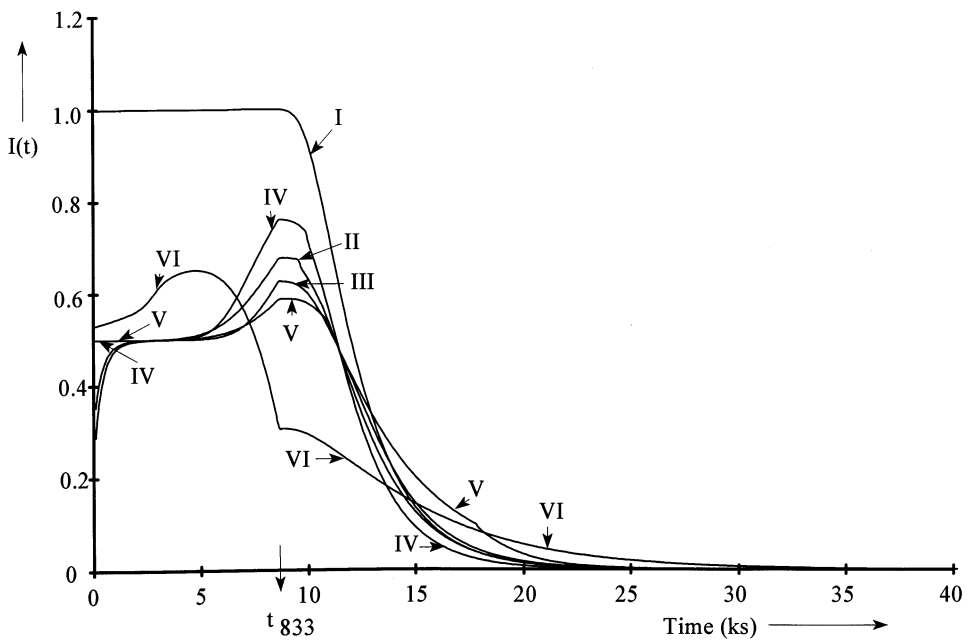

Fig. 9. The evolution of the inhomogeneity parameter for different initial concentrations. The curves are explained in the text and in Table 1. The homogenisation temperature was reached at $it_{833} = 8.66$ ks.

To distinguish between cases of zero and non-zero initial matrix concentrations, the Mg concentration has been set to zero for curves IV and V in Figs. 8 and 9. It can be observed that now the inhomogeneity parameter equals 0.5 at the early stages of the dissolution process. For later stages the difference in the behaviour of the inhomogeneity parameter decreases. For curves I–V the Mg_2Si-layer dissolves completely. The discontinuities of the inhomogeneity parameter are here caused by the transformation of the Dirichlet condition into a homogeneous Neumann condition when the Mg_2Si-layer disappeared.

For curve VI the initial matrix concentration of both alloying elements was set equal to 1 mass%. It can be seen that now the interfacial concentrations of both alloying elements are smaller than unity and the Mg_2Si-layer starts to grow (see Fig. 8). From Fig. 9 it can be seen that the inhomogeneity parameter for curve VI

Table 2
The values used for the initial matrix concentrations in the second set of calculations with varying initial matrix concentration and the indexing of the curves in Figs. 10 and 11

Curve index	c^0_{Mg} (mass%)	c^0_{Si} (mass%)	$M_2-S(0)$ (m)	T_{eq} (K)	$K(T_{eq})$
I	0.449×10^{-5}	0.993	2.542×10^{-7}	400	2.002×10^{-11}
II	0.399×10^{-3}	0.993	2.539×10^{-7}	500	1.58132×10^{-7}
III	0.793×10^{-2}	0.997	2.475×10^{-7}	600	6.2718×10^{-5}
IV	0.15229	1.0727	1.2537×10^{-7}	750	0.02488
V	0.22889	1.1128	6.04049×10^{-8}	775	0.05383

The symbols are explained in the text.

starts well under unity. This is caused by the large difference in the diffusion coefficients between Si and Mg at low temperatures. The inhomogeneity parameter of curve VI shows a discontinuity of its time derivative when the temperature reaches its maximum. As the temperature reaches its maximum, the solubility product stops increasing and reaches its maximum too, hence the inhomogeneity parameter for curve VI shows a discontinuity of its time derivative. For the case of growth (curve VI in Figs. 8 and 9) the compound layer grows until an equilibrium size is reached. When this equilibrium size is reached, the concentration gradients are zero. So, also for the case of a growing compound, matrix homogeneity is reached after a sufficient length of time.

3.5. The effect of initial matrix concentration at a fixed overall composition

The second set of calculations illustrates the influence of the initial matrix concentration on the dissolution kinetics. The overall concentration of both alloying elements are constant and equal to those of the reference system. To keep the overall concentrations constant, the thickness of the compound layer has been adjusted accordingly. The initial concentrations in the matrix and initial Mg_2Si-layer thickness correspond to equilibrium conditions at several temperatures. These conditions for which the equilibrium is reached at temperature T_{eq} may result during cooling after solidification. The configurations that have been used as the input for the simulations have been summarised in Table 2. As in the reference system, Eqs. (8a), (8b) and (8c) is used for the determination of c^0_{Mg}, c^0_{Si} and $M_2-S(0)$.

The results of the calculations with the input in Table 2 are given in Figs. 10 and 11. Fig. 10 displays the dissolution kinetics of the Mg_2Si-layer.

Curves I and II in Fig. 10 look like the reference system due to the low initial matrix concentrations and (almost) equal the initial shell thickness. Curves III, IV and V show a significant stage of growth at the early stages during the heat-up. Now the interfacial concentrations are significantly smaller than the initial concentration. This growth appears more pronounced for higher T_{eq}, as both the stage of growth is larger and the initial Mg_2Si-layer volume is smaller. For the cases in which subsequent growth and dissolution takes place, the concentration gradients of the alloying elements are zero at the maximum volume of the compound layer in Fig. 10. Now it is necessary to arrange Eq. (6) into a zero-point problem such that a division by a ('numerically') zero concentration gradient is avoided. This has been described in Ref. [17].

The inhomogeneity parameter (Fig. 11) shows an increase for curve I. In spite of an almost identical dissolution curve for condition II as for I in Fig. 10, its corresponding inhomogeneity parameter differs strongly. At the very early stages the Mg_2Si-layer grows. However, as this growth can only occur at the temperatures $T<T_{eq}=500$ K, in which the diffusion coefficients of the alloying elements are very small, the growth is negligible, but does have consequences on the behaviour of the inhomogeneity parameter. At the point of changing from growth into dissolution, the concentration profile becomes flat: the inhomogeneity parameter equals zero. Due to the Arrhenius relationship for the solubility product, the evolution of the interfacial concentrations seems to be sufficiently slow (for $T<T_{eq}$) to keep the minimum of the concentration at the moving boundary. This behaviour is observed for curves II–IV. However, for curve V, the inhomogeneity parameter does not touch the horizontal axis during the change of growth into dissolution in Fig. 11. This is due to the large increase in the interfacial concentrations with time at higher temperatures. In this case the application of the maximum principle of the diffusion equation allows for the existence of a local minimum of the concentration away from the moving boundary.

3.6. The effect of initial concentration profiles in the matrix at a fixed total concentration

The third set of calculations shows the influence of the shape of the initial matrix concentration profile. The initial concentration profiles shown in Fig. 12 have been used as the starting conditions. These concentration profiles resemble those obtained in practice with an

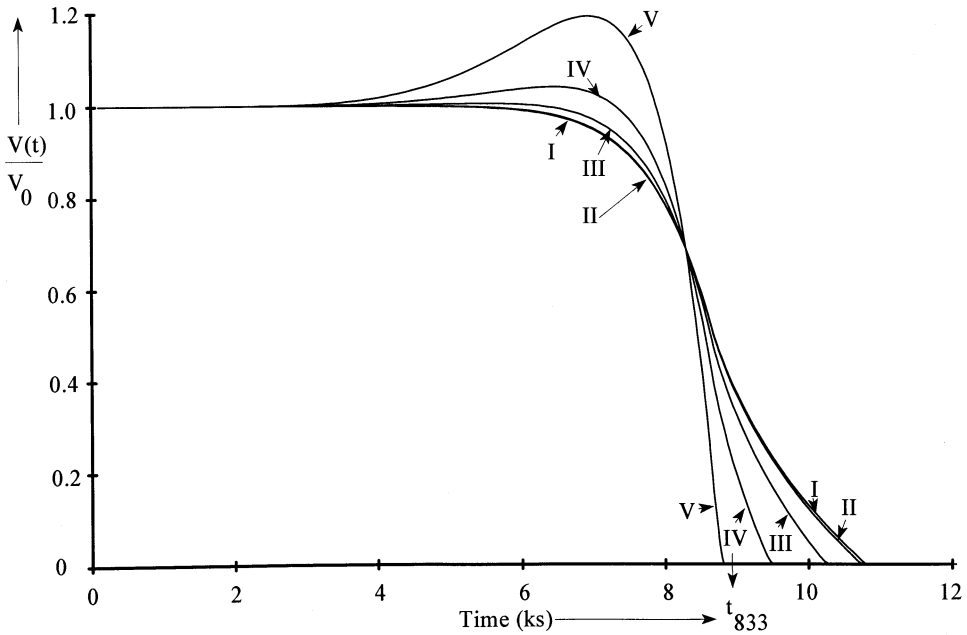

Fig. 10. The dissolution kinetics of a Mg_2Si-layer for different initial concentrations. The curves are explained in the text and in Table 2. The homogenisation temperature was reached at $t_{833} = 8.66$ ks.

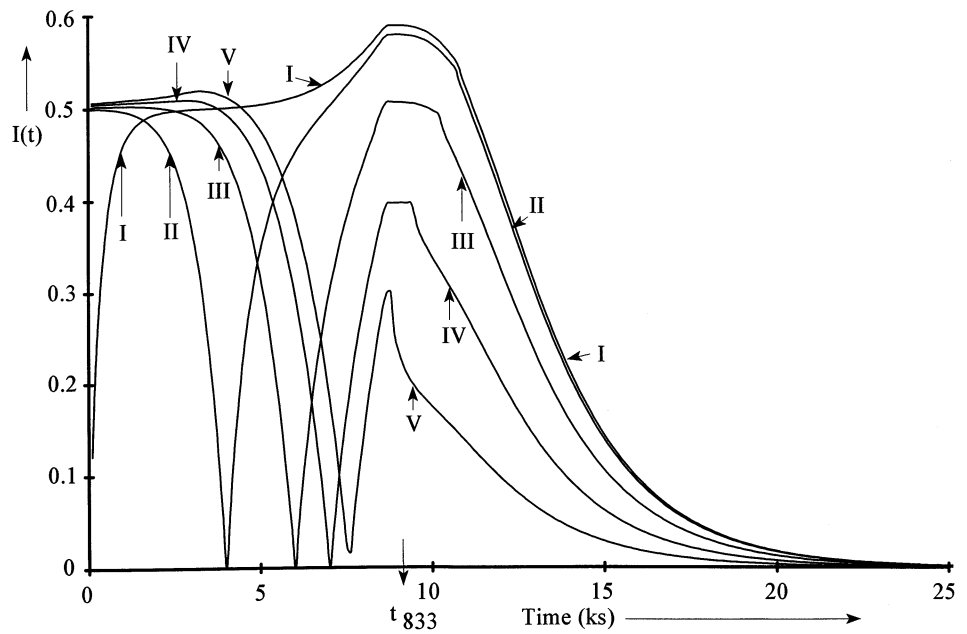

Fig. 11. The evolution of the inhomogeneity parameter for different initial concentrations. The curves are explained in the text and in Table 2. The homogenisation temperature was reached at $t_{833} = 8.66$ ks.

increasing cooling rate after solidification. In all calculations the same overall composition is used, i.e. the initial compound layer thickness has been adjusted accordingly and all other conditions are identical to those of the reference system. Curves I–V in Fig. 12, respectively, indicate the initial concentration profiles corresponding to an initial Mg_2Si-layer thickness of 3.251×10^{-8}, 3.607×10^{-8}, 4.12×10^{-8}, 4.9661×10^{-8} and 6.763×10^{-8} m. The results of the calculations for these initial matrix concentration profiles are given in Fig. 13. The normalised volume of the compound layer, $V(t)/V_0$, as represented by curves Ia–Va in Fig. 13, respectively, results from the initial concentrations I–V in Fig. 12. The corresponding evolution of the inhomogeneity parameter is depicted by curves Ib–Vb, respectively.

The initial concentrations used in these calculations do not represent thermodynamic equilibrium: the Mg_2Si-layer has had no time to grow to its equilibrium size. The average matrix concentrations of Si and Mg

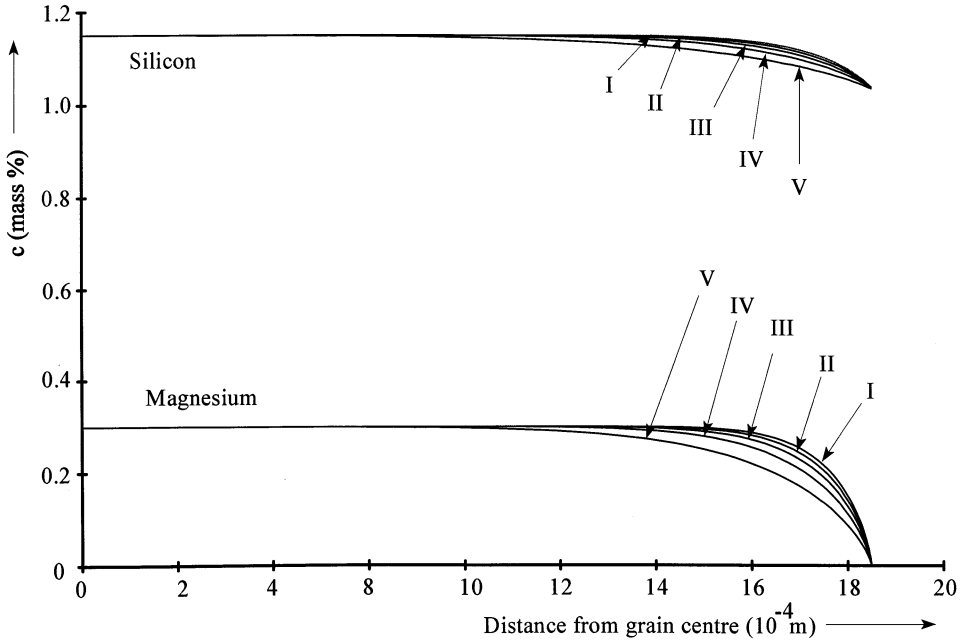

Fig. 12. The initial matrix concentration profiles used for the dissolution of the Mg_2Si-layer. The curves are explained in the text.

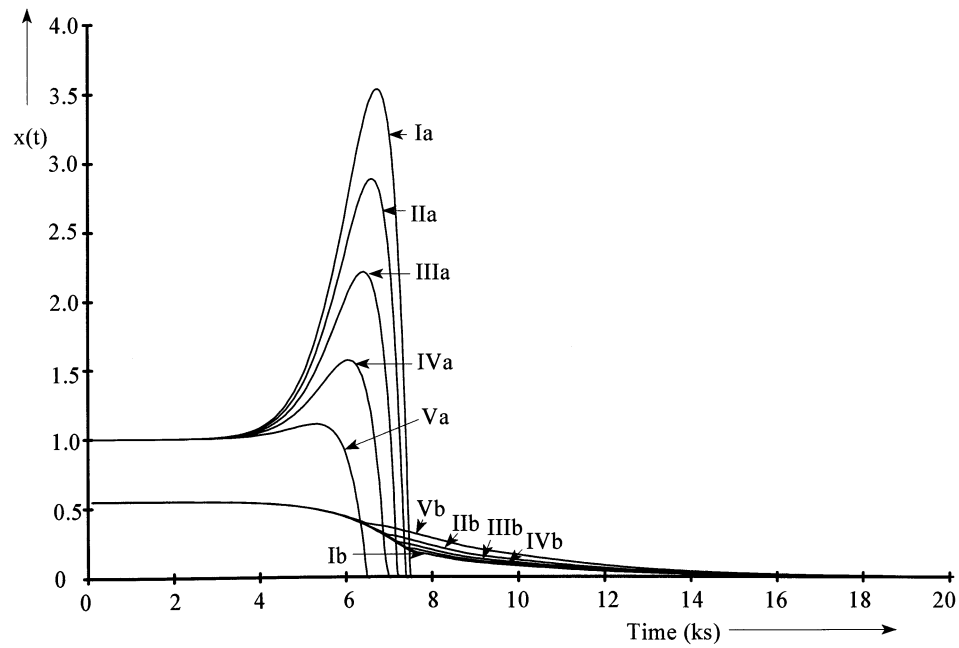

Fig. 13. The evolution of the dissolution kinetics and the inhomogeneity parameter for different initial concentrations from Fig. 12. The curves are explained in the text. The homogenisation temperature was reached at $t_{8.86} = 8.66$ ks.

respectively are larger than $c^0_{Si} = 0.993$ mass and $c^0_{Mg} = 0.2539 \times 10^{-5}$ mass fractions, corresponding to thermodynamic equilibrium for $T = 400$ K. Therefore, at the early stages of the heat-up, the layer of Mg_2Si grows. At the later stages, the temperature is high enough for the layer of Mg_2Si to dissolve. Fig. 13 shows that the concentration gradient at the interface influences the rate of dissolution severely. The evolution of the inhomogeneity parameter seems to be influenced by the concentration gradient at the interface as well.

3.7. The effects of the geometry of the second phase

The secondary phases in an alloy may have different geometries. The current model is valid for a dissolving sphere, cylinder, plate and a dissolving spherical/cylindrical layer of Mg_2Si (i.e. one-dimensional geometries). The initial 'thickness' of the dissolving second phase has been chosen equal, which means that for the spherical particle, cylindrical and planar phase $S(0) = 0.2542 \times 10^{-6}$ m and for the case of a spherical

compound layer $M_2 - S(0) = 0.2542 \times 10^{-6}$ m. The cell volume, however, has been adjusted such that the overall concentrations of the alloying elements are equal. All cases considered here thus correspond to the same initial second phase volume fraction of $f = 0.004615$. Table 3 shows the cell sizes used for the various geometries.

The results of the evolution of the precipitate volume and matrix inhomogeneity are shown in Figs. 14 and 15, respectively.

For the situation considered here, a fixed initial thickness of the dissolving particle has been used. The highest rates occurring for spherical particles are due to the more rapid decrease of the interfacial area during dissolution and the radially increasing diffusion space from the spherical interface. For planar geometry, the decrease in the interfacial area is zero, therefore causing a slower dissolution kinetics than for either a cylinder or a sphere. For a spherical Mg_2Si-layer, the interfacial area increases during dissolution and the diffusion space decreases radially from the interface towards the centre. From such facts it can be argued that different geometries of a secondary phase present in a material may dissolve at different rates. Note from Fig. 14 that the spherical and cylindrical particles entirely dissolve before the homogenisation temperature is reached.

It appears from Fig. 15 that the evolution of the inhomogeneity parameter varies equally strongly with geometry as well.

It can be seen that the inhomogeneity parameter evolves similarly for all geometries at the very early stages. This is because hardly any accumulation of atoms at the Neumann boundary has occurred yet. As the atoms accumulate at the Neumann boundary, the inhomogeneity parameter decreases: the matrix becomes more homogeneous. It can also be observed that the discontinuity of the derivative of the inhomogeneity parameter is greatest for a spherical particle. This is due to the fact that for this geometry the atoms can diffuse in all directions (4π steradians). For a cylindrical geometry, the atoms may diffuse at the angle 2π. Whereas, for the planar geometry only one direction can be used and for the spherical layer of Mg_2Si all atoms diffuse to the centre. This thus causes the slowest dissolution and smallest discontinuity of the time derivative of the inhomogeneity parameter. Note from Fig. 15 that for the spherical and cylindrical particle the matrix is homogeneous before the homogenisation temperature is reached.

An alternative approach would be to keep the cell volume and overall composition fixed, hence adjusting the initial particle thickness.

Table 3
The cell sizes used in the calculations for different geometries and the indexing of the curves in Figs. 14 and 15

Curve index	Geometry	Cell size (m)
I	Spherical particle	1.53×10^{-6}
II	Cylindrical particle	3.74×10^{-6}
III	Flat plate	5.508×10^{-5}
IV	Spherical layer	1.65×10^{-4}

3.8. The influence of heating rate and temperature gradients in the furnace

Various heating rates and homogenisation temperatures are used in industry. Therefore the effects of the heating rate and the homogenisation temperatures are also analysed here. Apart from the heating rate and the homogenisation temperature the starting conditions are all identical to those of the reference system. For completeness, it is repeated that the analysis described in this section has been done for the case of a spherical grain surrounded by a dissolving layer of Mg_2Si. Figs. 16 and 17, respectively, display the dissolution kinetics and the evolution of the inhomogeneity parameter for different heating rates (and a fixed homogenisation temperature of 833 K).

Curves I–IV in Figs. 16 and 17, respectively, correspond to heating rates of 0.05, 0.04, 0.03 and 0.02 K s^{-1} ($= 180$, 144, 108 and 72 K h^{-1}).

From Fig. 16 it can be observed that the curves appear flatter at the initial stages for lower heat-up rates in the furnace. This is because dissolution sets in at about the same temperature for all the curves, however for the case of fast heating up, the temperature increases quickly, during which the diffusion coefficients and solubility product increase quickly as well. Therefore dissolution sets in rapidly. From the arrows in Fig. 16 it can be seen that the volume fraction dissolved at the time it took to reach the homogenisation temperature increases with decreasing heat-up rate. Let t^* be the minimal time at which the temperature equals the homogenisation temperature of 833 K. Fig. 18 shows the residual volume fraction at $t = t^*$, $V(t^*)/V_0$, and inhomogeneity parameter at $t = t^*$, $I(t^*)$, as a function of the heat-up rate in K s^{-1}. It can be seen that for very small heat-up rates the whole compound layer is already dissolved when the homogenisation temperature is reached. For infinitely fast heating, no dissolution has taken place when the homogenisation temperature is reached, hence the residual volume fraction converges to one. For lower rates the remaining volume fraction when the homogenisation temperature is reached converges to zero (Fig. 18).

It can be seen from Fig. 17 that the shape of the inhomogeneity curve looks rather similar for all heat-up rates. However, its peak height and the part of the curves after the peak is shifted significantly for different heat-up rates. The maximal values in Fig. 17 corre-

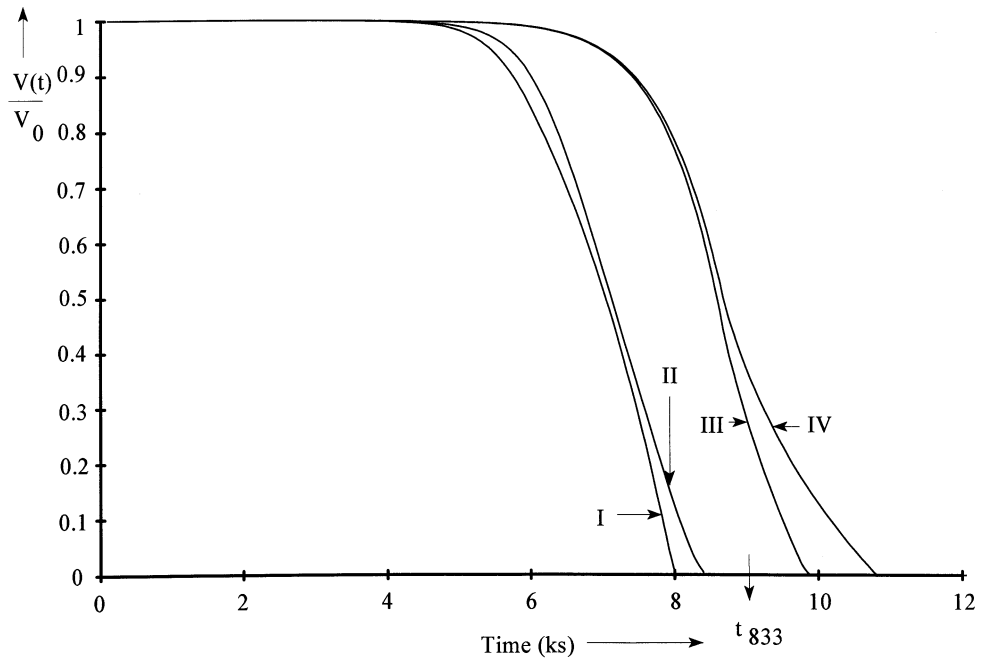

Fig. 14. The dissolution kinetics for different second phase geometries. The curves are explained in the text and Table 3. The homogenisation temperature was reached at $t_{833} = 8.66$ ks.

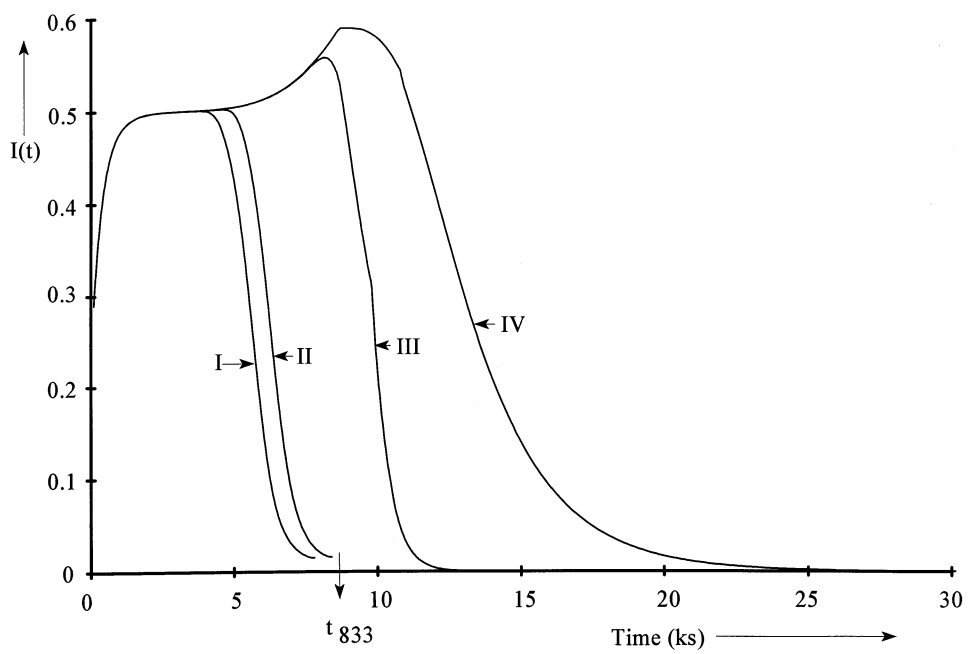

Fig. 15. The evolution of the inhomogeneity parameter for different second phase geometries. The curves are explained in the text and Table 3. The homogenisation temperature was reached at $t_{833} = 8.66$ ks.

spond to the values of the inhomogeneity parameter when the homogenisation temperature of 833 K is reached. Fig. 18 also displays the value of the inhomogeneity parameter when the homogenisation temperature is reached as a function of the heat-up rate. From Fig. 18 it is clear that for these cases when the compound layer dissolved entirely when the homogenisation temperature was reached (i.e. for very low heat-up rates), the inhomogeneity parameter is very low. This is attributed to the transition of the Dirichlet condition into a homogeneous Neumann condition when the boundary is fixed and to the atoms from the compound layer that have reached the grain centre when the temperature has reached the homogenisation temperature. For the fast heat-up rates no atoms from the Mg_2Si-layer have reached the grain centre yet when the

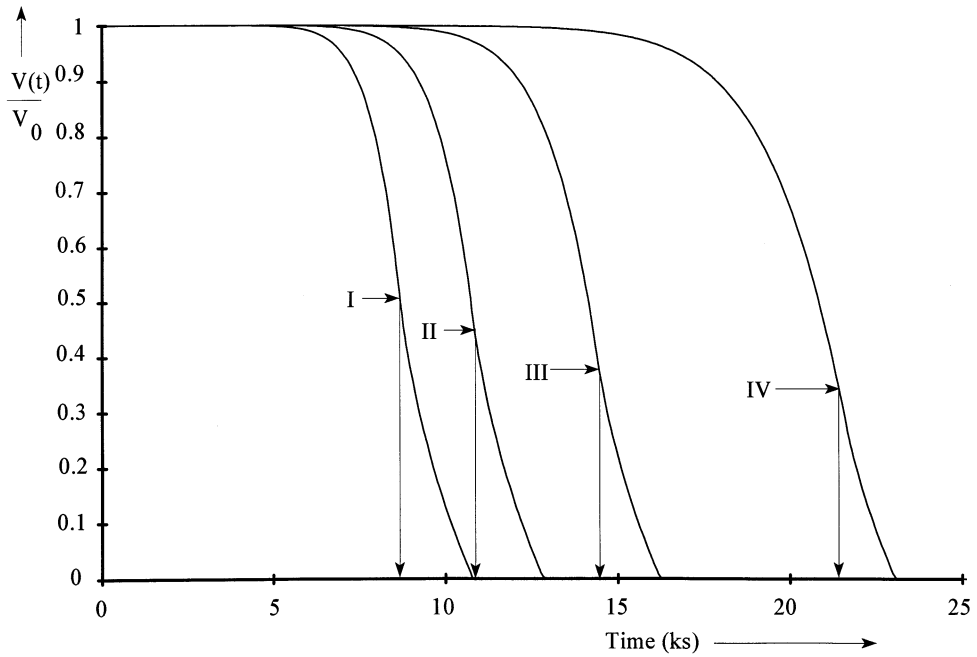

Fig. 16. The evaluation of the precipitate volume as a function of time for different heat-up rates. The curves are explained in the text. The vertical arrows indicate the time at which the homogenisation temperature for each curve was reached.

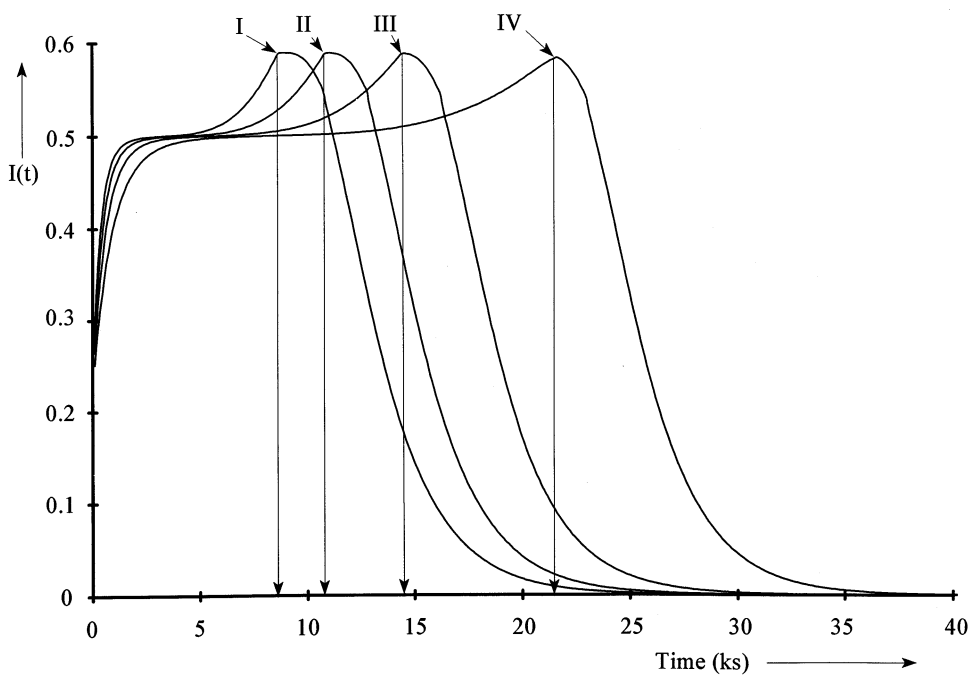

Fig. 17. The evaluation of the inhomogeneity parameter as a function of time for different heat-up rates. The curves are explained in the text. The vertical arrows for each curve indicate the time at which the homogenisation temperature was reached.

homogenisation temperature is reached, therefore the inhomogeneity parameter is about 0.58 (for the reference conditions selected) and does not vary with the heat-up rate. Note that the inhomogeneity parameters in Fig. 18 represent the maximum values for the inhomogeneity parameter as a function of time (viz. Fig. 17).

Similar results are shown in Figs. 19 and 20, in which curves I–V correspond to a heat-up rate of 0.05 K s^{-1} and different homogenisation temperatures of, respectively: 823, 813, 803, 793 and 783 K. The other conditions are identical to those in the reference system. The influence of persisting temperature gradients in the homogenisation furnace may be extracted from these curves. For curve III in Fig. 19 the layer dissolves completely in about 29 ks, its corresponding inhomo-

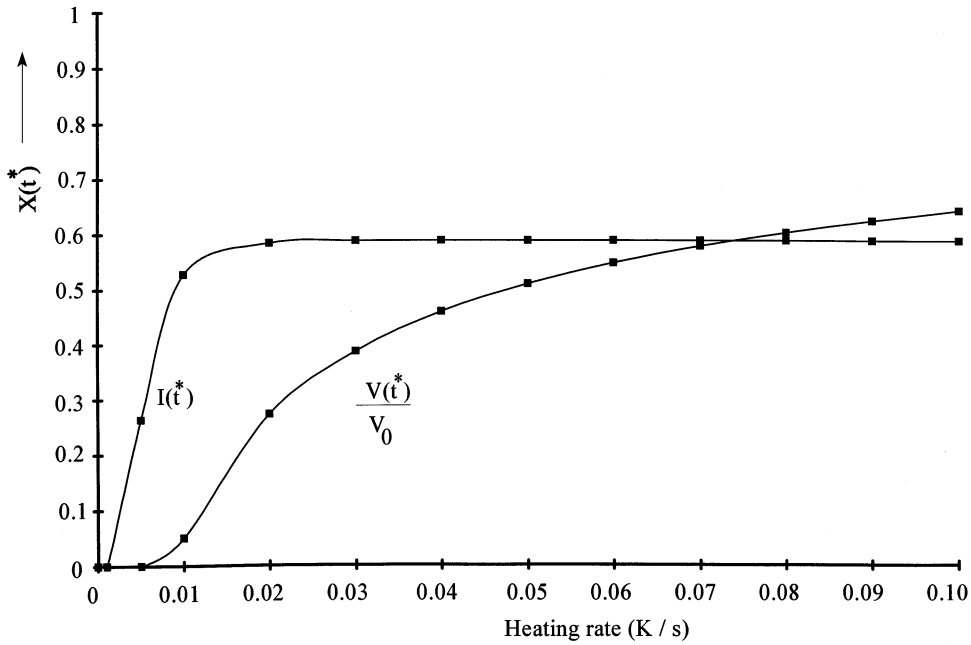

Fig. 18. The residual volume fraction and the inhomogeneity parameter when the homogenisation temperature of 833 K was reached as a function of the heating rate.

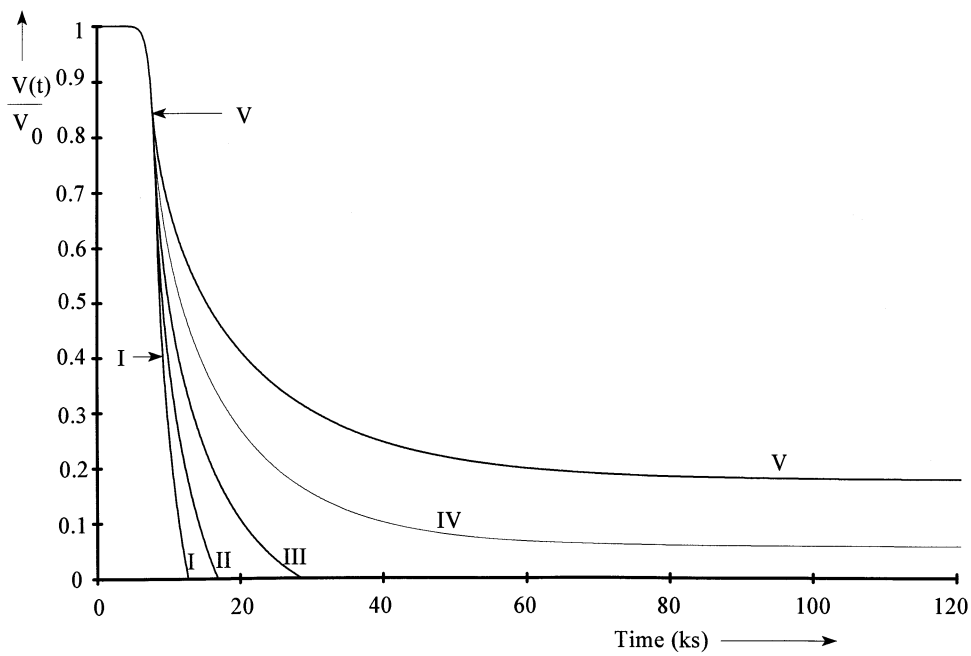

Fig. 19. The evolution of the volume of a dissolving Mg_2Si-layer for different homogenisation temperatures. The curves are explained in the text. The left-pointing and right-pointing arrows indicate the time at which the homogenisation temperature, of 823 and 783 K, respectively, were reached.

geneity parameter then shows a significant discontinuity in the time derivative (Fig. 20). It can be noted that the Mg_2Si-layer does not dissolve entirely for homogenisation temperatures of 793 and 783 K. However, it can be seen that the matrix composition becomes homogeneous for these cases as well (Fig. 20). In these cases it may also be observed from Fig. 20 that the inhomogeneity parameter does not show a discontinuity in its time derivative. Furthermore, it is observed that the position of the peak of the inhomogeneity parameter is approximately similar for all homogenisation temperatures. However, the peak becomes higher for higher homogenisation temperatures. Note from Fig. 19 that for a temperature of 803 K (curve III) the time needed for complete dissolution of the layer Mg_2Si-compound at the grain boundary is about twice the time needed

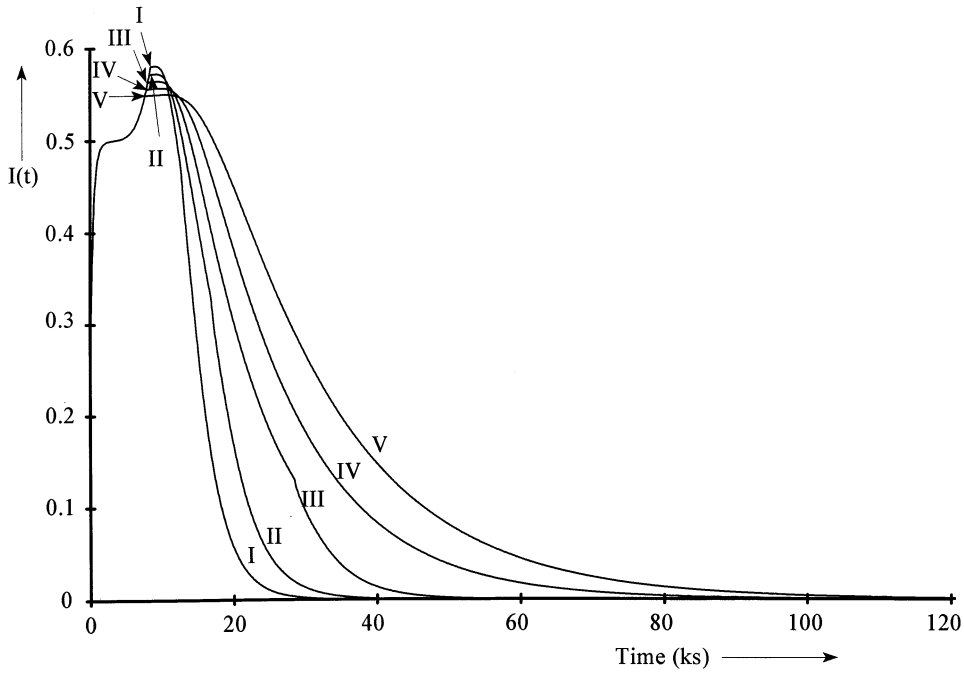

Fig. 20. The evolution of the inhomogeneity parameter for different homogenisation temperatures. The curves are explained in the text. The arrows indicate the time at which the homogenisation temperature was reached for each curve.

for complete dissolution at 823 K (a temperature difference of 20 K only!). Also, the time for complete matrix homogeneity is almost doubled. This means that in order to obtain similar qualities for temperatures 803 and 823 K, the homogenisation time required at a temperature of 803 K is about twice as long as the homogenisation time at a temperature of 823 K. This is due to the Arrhenius-like relationship of the diffusion coefficient and solubility product.

4. Discussion

The model presented here can be used to investigate the dissolution kinetics of second phases in ternary alloys. All one-dimensional geometries (sphere, cylinder, flat plate, cylindrical- and spherical-layer of a compound around the grain) can be dealt with. In reality, however, the grains are not strictly spherical but rather shaped like tetrakaidecahedrons (an ideal representation of a Voronoi-cell) (unpublished research), constituting a three-dimensional Stefan problem. For reasons of simplicity the ternary Stefan problem has been reduced to a one-dimensional problem.

To investigate the influence of the two-dimensional effects, a two-dimensional finite element method [4] has been used for the computation of the dissolution of a secondary phase layer around a hexagonal grain in a binary alloy. The same calculations were done for the dissolution of a layer of a secondary phase around a circular grain in a binary alloy using the finite volume method. The results differed about maximal 10% from the calculations using the finite volume method applied to the dissolution of a second phase layer around a circular grain. All numerical settings for both cases were chosen as similar as possible. The grain and secondary phase thickness were chosen so that the grain and secondary phase areas were equal for the hexagonal and circular geometry. For both cases considered here the discretisation of the moving boundaries was one-sided, i.e. the virtual gridpoints at the moving boundaries were omitted, causing a less accurate computation of the free boundary position.

The calculations on the effect of particle geometry were performed while keeping the initial thickness of the particle (and the overall concentration) constant. If, alternatively, the cell size is kept constant and the 'thickness' of the particle is adjusted to get the fixed overall composition, the order of dissolution times for the various geometries as shown in Figs. 14 and 15 reverses. Moreover the situation in which the cell volume and overall composition are fixed and two secondary phases are chosen in the cell such that their total volume is also equal, may be considered as well, for different initial thicknesses of the dissolving phases. An example of two simulateneously dissolving phases is given in Ref. [17]. Clearly the correct definition of the three-dimensional geometry and size of both the dissolving phase and that of the matrix is of

crucial importance for calculating the dissolution kinetics.

In the calculation of the dissolution kinetics of a second phase it was found for some cases that the second phase first grows and then dissolves subsequently. This implies that the concentration gradient of one or both alloying elements at the moving interface may be zero or 'numerically' zero (due to rounding errors in the computer arithmetic). The re-arrangement of Eqs. (5) and (6) into a zero-point problem has therefore been done so that no division by the concentration gradients of the alloying elements at the interface takes place during the calculations. If this is not done properly, severe numerical instabilities during the modelling of subsequent growth and dissolution may arise.

The influence of the presence of (dissolving) precipitates inside the grain on the dissolution kinetics of a layer of Mg_2Si at the grain boundary is very complex due to the possible spatial distribution of the locations of the particles. The current model may be used to provide an estimate for this effect by positioning a precipitate in the centre of the grain. Simultaneous dissolution of these secondary phases then can be dealt with using a two-moving boundary problem in a ternary alloy. The numerical details and influences have been described in Ref. [17].

5. Conclusion

The evolution of the microstructure during the homogenisation treatment of aluminium alloys depends on the shape of the statistical distribution of the size of the second phase, the geometry of the second phase, alloy composition, initial matrix concentration profiles of the alloying and the temperature–time profile during the homogenisation treatment.

The concentration gradients in the matrix disappear long after the dissolution of the second phases.

Appendix A. On the local curvatures of the $I(t)$-curve during the heating stage

From the differentiation of Eq. (7) it follows that the time derivative of the inhomogeneity parameter is given by (in which we used respectively $x_p(t)$ and $y_p(t)$ to indicate $\max_{r\in G(t)}(c_p(r,t))$ and $\min_{r\in G(\mathrm{it})}(c_p(r,t))$. Note that these quantities here are respectively given by $c_p[S(t),t]$ and $c_p(0,t)$):

$$\frac{\mathrm{d}I(t)}{\mathrm{d}t}=\frac{1}{2}\cdot\sum_{p\in\{\mathrm{Mg,Si}\}}\left(\frac{y_p(t)}{x_p^2(t)}\frac{\mathrm{d}x_p(t)}{\mathrm{d}t}-\frac{1}{x_p(t)}\frac{\mathrm{d}y_p(t)}{\mathrm{d}t}\right)\quad\text{for } x_p(t)\geq y_p(t)\geq 0,\ t>0. \tag{A1}$$

By differentiating once more, it is obvious that:

$$\frac{\mathrm{d}^2I(t)}{\mathrm{d}t^2}=\frac{1}{2}\cdot\sum_{p\in\{\mathrm{Mg,Si}\}}\left[\frac{[x_p'(t)y_p'(t)+y_p(t)x_p''(t)]\cdot(x_p(t))^2-2x_p(t)y_p(t)x_p'(t)}{(x_p(t))^4}\right]-\frac{1}{2}\cdot\sum_{p\in\{\mathrm{Mg,Si}\}}\frac{y_p''(t)x_p(t)-x_p'(t)y_p'(t)}{(x_p(t))^2}. \tag{A2}$$

For the stages in which the atoms from the Mg_2Si-layer did not reach the grain centre, i.e. $y_p(t)=c_p^0(M_1=0)$, the above expression can be written as:

$$\frac{\mathrm{d}^2I(t)}{\mathrm{d}t^2}\approx\frac{1}{2}\cdot\sum_{p\in\{\mathrm{Mg,Si}\}}\left[y_p(t)\frac{x_p''(t)(x_p(t))^2-2x_p(t)x_p'(t)}{(x_p(t))^4}\right]. \tag{A3}$$

From Eq. (1) and Fig. 1, it follows that in the early stages

$$\frac{y_p(t)}{x_p^2(t)}\frac{\mathrm{d}x_p(t)}{\mathrm{d}t}>0$$

due to the heat-up and

$$\frac{1}{x_p(t)}\frac{\mathrm{d}y_p(t)}{\mathrm{d}t}\approx 0$$

as long as $\pi D_p t<(S_2(t)-S_1(t))^2)$, in which the minimum concentration hardly changes, we have $(\mathrm{d}I(t)/\mathrm{d}t)>0$. As, at the early stages, $x_p(t)<1$ and even $x_{\mathrm{Mg}}(t)\ll 1$, we have $(x_p(t))^2<x_p(t)\approx y_p(t)$ and therefore $\mathrm{d}I(t)/\mathrm{d}t$ becomes large. From a finite difference differentiation of $x_p(t)$ and $y_p(t)$, the quantities $x_p'(t)$, $y_p'(t)$, $x_p''(t)$ and $y_p''(t)$ have been determined. Substitution of these values into Eq. (A3), reveals that for $t<3.2$ ks, we have $\mathrm{d}^2I(t)/\mathrm{d}t^2$. Due to the larger variation of the solubility product and the diffusion coefficients for higher temperatures, $\mathrm{d}x_p(t)/\mathrm{d}t$ increases more rapidly with time (as $(\mathrm{d}^2x_p(t)/\mathrm{d}t^2)>0$, see also Fig. 1), substitution of the quantities $x_p(t)$, $y_p(t)$, $x_p'(t)$, $y_p'(t)$, $x_p''(t)$ and $y_p''(t)$ into Eq. (A3), yields $(\mathrm{d}^2I(t)/\mathrm{d}t^2)>0$ for $t>3.3$ ks. $I(t)$ thus has a point of inflection for some $t\in(3.2,\ 3.3\ \mathrm{ks})$.

References

[1] M.J. Whelan, Met. Sci. J. 3 (1969) 95.
[2] U.L. Baty, R.A. Tanzilli, R.W. Heckel, Met. Trans. 1 (1970) 1651.
[3] U.H. Tundal, N. Ryum, Met. Trans. 23A (1992) 433.

[4] G. Segal, C. Vuik, F.J. Vermolen, J. Comp. Phys. 141 (1998) 1.
[5] F.J. Vermolen, P. van Mourik, S. van der Zwaag, Met. Sci. Technol. 13 (1997) 308.
[6] F.V. Nolfi Jr., P.G. Shewmon, J.S. Foster, Trans. Met. Soc. AIME 245 (1969) 1427.
[7] H.B. Aaron, G.R. Kotler, Met. Trans. 2 (1971) 393.
[8] F.J. Vermolen, S. Van der Zwaag, Mater. Sci. Eng. A220 (1996) 140.
[9] G.P. Krielaart, PhD thesis, Delft University of Techology, 1995.
[10] J. Ågren, J. Phys. Chem. 43 (1981) 421.
[11] J.M. Vitek, S.A. Vitek, S.A. David, Met. Mater. Trans. A 26A (1995) 2007.
[12] R. Hubert, ATB Metall. 34, 35 (1995) 5–10.
[13] O. Reiso, N. Ryum, J. Strid, Met. Trans. 24A (1993) 2629.
[14] J. Kaneko, M. Mokhtar Sultan, R. Horiuchi, Z. Metallk. 67 (1976) 8.
[15] L. Lodgård, N. Ryum, Precipitation of dispersoids in a 6062 alloy, in: Proc. 5th Conf. on Advanced Materials and Processes and Applications vol. 4, EUROMAT, Maastricht, the Netherlands, 1997.
[16] F.J. Vermolen, C. Vuik, S. van der Zwaag, Mater. Sci. Eng. A (1998) in press.
[17] F.J. Vermolen, C. Vuik, A numerical method to compute the dissolution of second phases in ternary alloys, Internal Report for the Faculty of Technical Mathematics and Informatics, Delft University of Technology, J. Comput. Appl. Math. (accepted).
[18] J. Aitchinson, J.A.C. Brown, The Lognormal Distribution: with Special Reference to its Uses in Economics, Cambridge University Press, Cambridge UK, 1976.
[19] F.J. Vermolen, H.M. Slabbekoorn, S. van der Zwaag, Mater. Sc. Eng. A230 (1997) 80.
[20] C.J. Keuhmann, P.W. Voorhees, Met. Trans. 27A (1996) 937.
[21] D.A. Porter, K.E. Easterling, Phase Transformations in Metals and Alloys, Chapman and Hall, London, 1991.
[22] S. Fujikawa, K. Hirano, Y. Fujikawa, Met. Trans. 9A (1978) 1811.
[23] Y. Minamino, T. Yamane, A. Shimomura, et al., J. Mater. Sci. 18 (1983) 2679.
[24] J. Crank, Free and Moving Boundary Problems, Clarendon Press, Oxford, 1984.
[25] Y. van Leeuwen, J. Sietsma, S. Vooijs, S. van der Zwaag, The effect of geometrical assumptions in modelling the transformation kinetics for massive transformations, Met. Mater. Trans. A (1998) (submitted).

$c_{Si}[S(t), t]$, is obtained from Eq. (5). The iteration procedure to obtain the Dirichlet concentrations at the moving boundaries in each cell, such that the concentration profiles of both alloying elements satisfy Eqs. (2)–(6), is done by the re-arrangement of Eq. (6) such that a zero-point problem results. The roots are determined using a discrete Newton–Raphson procedure. This is repeated until the desired accuracy is reached. More details about the numerical solution procedures can be found in Ref. [17].

Using these two Dirichlet boundary conditions at the moving boundary, the diffusion equations for both alloying elements, Eq. (1), are solved using a finite volume method with a geometrically divided grid, i.e. between subsequent integration nodes $i-1$, i and $i+1$ we have $r_{i+1}-r_i=\alpha(r_i-r_{i-1})$. A geometrically divided grid allows local mesh refinement and coarsening and thus improves the efficiency of the calculation. The whole concentration profile is determined using virtual gridpoints at the boundaries to guarantee a global accuracy of $O(\Delta r^2)$. In case of fixation of a moving boundary, i.e. $S(t)=M_m$, the Dirichlet boundary condition changes into a homogeneous Neumann boundary condition.

The above described scheme is carried out for each time-step. At each time-step the gradient at the interface from the concentration profile obtained is used to determine the displacement of the interface (i.e. Eq. (6)). After the determination of the new interfacial position, the mesh is adjusted so that the interface coincides with the same gridpoint during the whole simulation. Subsequently the concentration profile at the new points are determined using a linear interpolation (i.e. a convective derivative).

This whole iteration procedure is done until:

$$\frac{1}{2}\sum_{p\in\{\mathrm{Mg,Si}\}}\left\{\frac{\max_{r\in G(t)}(c_p(r,t))-\min_{r\in G(t)}(c_p(r,t)}{\max_{r\in G(t)}(c_p(r,t))}\right\}<\delta,$$

with arbitrarily $\delta=10^{-5}$ and $G(t)$ denotes the matrix domain, $G(t)\equiv\{r\in R|0\le r\le S(t)\le M_2\}$, for a dissolving secondary phase at the grain boundary and $G(t)\equiv\{r\in R|0\le S(t)\le r\le M_2\}$ for a dissolving particle at the grain centre.

3. Results

Some calculations have been done to highlight the influence of several industrially relevant parameters: the grain size distribution, the initial Mg and Si concentrations in the matrix, the second phase geometry and local temperatures in an industrial furnace. The results of the calculations show the evolution of the second phase volume and the matrix inhomogeneity as a function of time. The matrix inhomogeneity has been quantified using the so-called dimensionless inhomogeneity parameter, $I(t)$. This parameter is a measure for the maximum concentrational difference in the matrix relative to the maximum of the concentration present in the matrix, $G(t)$, at time it. This parameter has been defined as follows:

$$I(t)\equiv\frac{1}{2}\sum_{p\in\{\mathrm{Mg,Si}\}}\left\{\frac{\max_{r\in G(t)}(c_p(r,t))-\min_{r\in G(t)}(c_p(r,t))}{\max_{r\in G(t)}(c_p(r,t))}\right\},$$
$$\text{with } \max_{r\in G(t)}(c_p(r,t))\ge\min_{r\in G(t)}(c_p(r,t))\ge 0 \qquad (7)$$

$I(t)$ ranges from unity (corresponding to the situation where $\max_{r\in G(t)}(c_p(r,t))>\min_{r\in G(t)}(c_p(r,t))=0$, i.e. the concentrations at the moving (Dirichlet) interface and fixed (Neumann) boundary, respectively, are non-zero and zero) to zero (corresponding to the situation where $\max_{r\in G(t)}(c_p(r,t))=\min_{r\in G(t)}(c_p(r,t))$, i.e. uniform concentration profiles of both alloying elements).

3.1. The idealised reference system

First an idealised reference system in which a spherical layer of Mg_2Si dissolves in a spherical grain has been chosen. The presence of other (Si-rich) phases has been excluded. This reference system is then used to illustrate the influences of all model parameters separately. The reference system represents an AlMgSi-alloy with an average Mg concentration, $\langle c_{Mg}\rangle=0.3$ mass% and an average Si concentration, $\langle c_{Si}\rangle=1.15$ mass% and a grain radius $M_2=1.65\times10^{-4}$ m. The concentrations of Mg and Si in the Mg_2Si compound layer are, respectively, $c_{Mg}^{part}=65$ and $c_{Si}^{part}=35$ mass%. The alloy is assumed to be heated from 400 to $T_{hom}=833$ K with a heating-rate of 0.05 K $s^{-1}=180$ K h^{-1}. Initially, the thickness of the compound layer and matrix concentrations are chosen such that they correspond to thermodynamic equilibrium at 300 K. The hyperbolic relationship (see Eq. (5)) has been assumed to be valid for this combination of compositions and equilibrium temperature. The solubility product, $K(T)$, has been determined from the thermodynamic software package MTDATA (MTDATA is a commercial software package for multicomponent thermodynamics developed at the National Physical Laboratory, London).

The initial matrix concentrations of both alloying elements, c_{Mg}^0, c_{Si}^0 and initial second phase volume fraction, f, are related to the above given data by:

$$c_{Si}^0(1-f)+c_{Si}^{part}f=\langle c_{Si}\rangle, \qquad (8a)$$

$$c_{Mg}^0(1-f)+c_{Mg}^{part}f=\langle c_{Mg}\rangle, \qquad (8b)$$

$$(c_{Si}^0)(c_{Mg}^0)=K(T=300\text{ K})=6.4\times10^{-12}(\text{mass\%})^3. \qquad (8c)$$

The above system is solved to yield c_{Mg}^0, c_{Si}^0 and the Mg_2Si volume fraction. For the selected overall composition and equilibrium temperature, this yields: $c_{Mg}^0=2.539\times10^{-6}$ mass%, $c_{Si}^0=0.993$ mass and $f=0.004615$